Analysis of Blockage Effects on Roadside Relay-assisted mmWave Backhaul Networks

Yuchen Liu and *Douglas M. Blough*
School of Electrical and Computer Engineering, Georgia Institute of Technology, Atlanta, GA, 30332

***Abstract*—mmWave communication is a highly promising technology for 5G wireless backhaul. However, network performance is hard to predict due to the sensitivity of mmWave signals to blockages. In this paper, we propose an analytical framework to incorporate blockage effects and evaluate blockage robustness within a previously proposed interference-free topology for roadside relay-assisted mmWave backhaul. Through stochastic geometric analysis, the blockage probabilities for four types of blockages identified in prior work are derived as a function of the topology parameters and obstacle density. Analysis of the effect of topology parameters on blockage probability yields insight that leads to a modified topology, which maintains the desirable interference-free property but has better blockage robustness than the original topology. Simulation results demonstrate that the modified topology can maintain very high throughput and has significantly improved robustness as compared to the original topology, while using the same number of relays.**

I. Introduction

With the advent of fifth generation wireless networks, millimeter wave (mmWave) communication is a key enabling technology for various bandwidth-hungry applications and scenarios. A promising use case is wireless backhaul [1], [2], where small-cell base stations (BSs) form a mesh or tree network to carry data traffic among themselves and to/from a macro-cell BS without any wired connections. However, the higher path loss and sensitivity to blockages of mmWave communications are two challenges that must be overcome for its full potential to be realized. Thanks to the shorter wavelength, large-scale phased antenna arrays with high-gain directivity can be applied to help compensate the poor propagation characteristics of mmWave signals. However, blockage effects can still prevent communication on line-of-sight (LOS) paths in the mmWave band and non-LOS paths can have very high energy loss, which makes it difficult to predict and analyze the performance of mmWave networks [3].

To handle blockage problems and increase coverage, some research uses relays to maintain connectivity for mmWave networks in outdoor environments, where a sequence of relatively short but very high rate mmWave links combine to produce a long-distance high-rate mmWave path. This use case is very well suited for the backhaul mesh links [4], because mmWave paths with relays can be reconfigured dynamically to avoid temporary blockages like vehicles [5], and can extend the range of wireless backhaul communications. In previous works, several relay selection algorithms for multi-hop settings and mmWave backhaul have been studied [4], [6], which aim to achieve high-throughput without considering blockages. In [7], a MAC protocol is presented, which can overcome blockage problems using a single relay. In [8], an opportunistic relay selection scheme to minimize outage probability is proposed, but this work does not study randomly placed obstacles, which is the subject of this paper.

Blockage modeling has traditionally been incorporated into the shadowing model as a log-normal distributed random variable, but this approach does not capture the distance-dependence of blockage effects, since more shadowing should be experienced over the longer link intuitively. For mmWave signals, stochastic geometry is an important mathematical tool to characterize random obstacles and provide acceptable estimation of blockage effects with only a few parameters [9]. For performance analysis in mmWave networks, there are three main stochastic geometry urban models. The first one is the Poisson-line model [10], where urban areas or obstacles are modeled by the parameters of the line process. However, our study focuses on roadside environments where large vehicles are viewed as the main obstacles, and line segments can not model this kind of blockage well because a vehicle's width affects the blockage conditions. The second model is called the LOS-ball model [11], where a link between two nodes has a LOS only if the separation distance is shorter than a given threshold, and it substantially simplifies the performance analysis, but loses an elaborate geometric description of blockage objects. Compared with these two simplified models, the Boolean model is more suitable for our roadside scenario. In the Boolean model, obstacles with random sizes are rectangularly distributed in a plane based on random shape theory. [12], [13] use this model to analyze the blockage effects on urban cellular networks, but ignores the correlated blockage for multiple nearby links, which needs to be considered in our roadside relaying topology.

In this paper, we study blockage effects in relay-assisted mmWave backhaul networks, where mmWave relays are deployed on regularly-spaced lampposts according to a *triangular-wave topology* [14]. However, these deployments could be susceptible to obstacles in the form of large trucks or other objects that could block some of the LOS paths between consecutive nodes. An example of this scenario is shown in Fig. 1. Thus, it is necessary to analyze the correlation between blockages and mmWave paths, which is closely related to the network robustness. In this paper, based on a previously proposed *four-type blockage model* [5], we introduce a mathematical framework to model random obstacles and analyze their impacts on different available links through stochastic geometry. The probabilities of different-type blockages are examined as a function of the topology angle, obstacle density and size. Then the impact of these parameters on blockage

978-1-5386-8088-9/19/$31.00 ©2019 IEEE

probability is investigated. This analysis leads us to propose a modification to the original triangular-wave topology, which we refer to as the *wide-end-angle triangular wave topology*. Through simulation, we demonstrate that blockage robustness is significantly improved for the wide-end-angle topology compared to the original topology, while end-to-end throughput and relay cost are nearly the same for these two topologies.

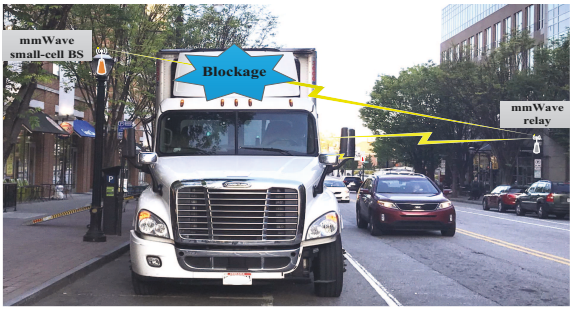

Fig. 1. A parked truck next to a lamppost in an urban environment.

II. System Overview

In this section, we introduce the topology, blockage, channel, and antenna models used in the remainder of the paper.

A. Topology and blockage model

The interference-free triangular-wave topology (IFTW) is very well suited to provide high data rate communications for relay-assisted mmWave backhaul in roadside environments [5], [14]. In the IFTW topology, BSs and relays (N_k) are deployed on equally-spaced lampposts on both sides of the road, where the topology angle θ and horizontal distance between adjacent nodes d_0 are the same everywhere along the topology (as depicted by the blue links of Fig. 2). One advantage of the IFTW topology is that the mutual interference along the path can be eliminated if θ is made large enough relative to the beamwidth ϕ of the directional antennas (Theorem 1 in [14]), i.e., if the interference-free condition in Eq. (1) is satisfied:

$$\theta - \arctan(\frac{\tan\theta}{3}) > \frac{\phi}{2}. \tag{1}$$

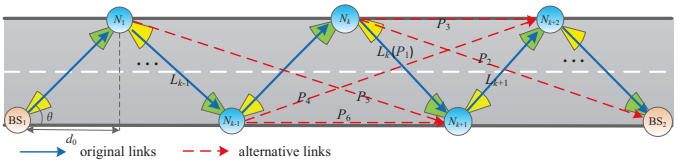

Fig. 2. Original and alternative links in the IFTW topology.

Given a road width d_w and length d_l, d_0 and the number of required nodes N (including two BSs and several relays) in the IFTW topology are only determined by θ as $d_0 = d_w/\tan\theta$ and $N = \lfloor d_l/d_0 \rfloor + 1$, respectively.

Another advantage of the IFTW topology is the ability to reconfigure mmWave paths to avoid obstacles that occur along the roadway. Through adaptive beam steering when an obstacle blocks one or more of the original links, alternative links (shown in Fig. 2) can be used to restore the connectivity of the topology. In our previous work [5], we identified the following four types of blockages that can occur from a single obstacle along the roadway with the IFTW topology:

a) Type I: An obstacle in L_k region blocks only a original link of the topology, such as P_1 in Fig. 2.

b) Type II: An obstacle in L_k region blocks an original link and an adjacent alternative diagonal link simultaneously, such as $\{P_1, P_2\}$ for N_k or $\{P_1, P_5\}$ for N_{k+1}.

c) Type III: An obstacle in L_k region blocks an original link and a crossing alternative diagonal link, such as $\{P_1, P_4\}$.

d) Type IV: An obstacle in L_k region blocks all the TX/RX links of N_k/N_{k+1}, such as $\{P_1, P_2, P_3\}/\{P_1, P_5, P_6\}$, which is equivalent to the failure of node N_k/N_{k+1}.

Any blockages produced by randomly placed obstacles can be decomposed into one or a combination of the above four types (Theorem 1 in [5]). This model takes into account the correlation between blockages, for example, a single blockage close to a node could block multiple mmWave paths simultaneously, which has not been considered in most previous studies. In what follows, we investigate an analytical framework and the spatial correlation of blocked links based on this blockage model in the IFTW topology.

B. Channel and antenna model

Here we make the standard assumption of additive white Gaussian noise channels. The rate of the directional unblocked link l follows Shannon's Theorem with an upper limitation, i.e.

$$R_l \le \beta \cdot B \cdot \log_2(1 + \min\{\frac{P_r(d)}{N_T}, T_{\max}\}), \tag{2}$$

where B is channel bandwidth, N_T is the power of thermal noise, T_{max} is the upper bound of operating signal-noise ratio due to the limiting factors like linearity in the radio frequency front-end, and the link utility ratio $\beta \in (0, 1)$. Considering the primary interference of our simplified relays, $\beta \le 0.5$. Here $P_r(d)$ is the received power of the intended transmitter's signal, and equals $k_0 P_t G_t G_r d^{-\alpha}$, where $k_0 \propto (\lambda_w/4\pi)^2$, λ_w is the signal's wavelength, d is the propagation distance, α is the path-loss exponent, and G_t and G_r are antenna gains at the transmitter and receiver, respectively.

To achieve the high rate requirement of mmWave backhaul, only nearby LOS neighbors of each node are considered as candidates to be selected for next hops. Therefore, only relatively short alternative links are considered for blockage avoidance (to be specific, only the 3 nodes immediately before or after a blocked original link in Fig. 2 are considered as possible transmitters or receivers for alternative links).

In this work, a flat-top directional antenna model is adopted, which means that transceiver antennas have a high constant gain G_h within the beam, and a very low gain G_l that can be ignored outside the narrow beamwidth ϕ. Interference due to reflections of the main beam and from side lobe emanations are not considered. Although it is outside the scope of this paper, it is not difficult to show that these effects have only a small impact on SINR in the considered network scenario.

III. Quantification of Blockage Effects

In this section, we give an mathematical analysis for blockage effects in our topology. Based on the four-type blockage

model, we first derive the different-type blockage probabilities in the single-obstacle case, and then extend to the general multi-obstacle case through stochastic geometric analysis.

A. Single-obstacle case

Under the single-obstacle situation, i.e., a single obstacle with random size would occur in the topology, some key assumptions should be made as follows:

Assumption 1: (*Constraint of Size*): A single obstacle can block at most two consecutive original links (e.g. L_k and L_{k+1} in Fig. 2), and its width must be less than the road width. This constraint is reasonable since vehicles cannot be large enough to affect links separated by several tens of meters.

Assumption 2: Obstacles are viewed as rectangles with random length and width. The center of the rectangle must fall within the road area, and follows the uniform distribution. The orientation θ_o of the obstacle is the same as the road's direction (i.e., θ_o equals the topology angle θ), because the vehicles always drive in the direction of road.

With these assumptions, the blockage areas in one of the original link regions of the topology are depicted in Fig. 3. Since only relatively short alternative links are considered for blockage avoidance, if the original link L_1 is blocked, each node has two kinds of alternative links: shorter-substitute link L_2 and longer-substitute link L_3, and their respective blockage areas are overlapping with each other due to the spatial correlation of blocked links. From this figure, we can see that the overlapping of different blockage areas is determined by the topology angle θ and the random obstacle's width w and length l within a specific road.

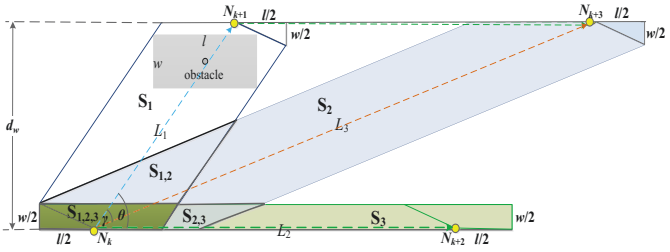

Fig. 3. Overlapping of blockage areas in one original link region.

Based on the four-type blockage model, we can first compute different-type blockage areas in one original link region. Firstly, the occurrence of *Type* I blockage indicates only original link L_1 is blocked, and an arbitrary rectangle (obstacle) $B(w,l,\theta)$ intersects the original link L_1 if and only if its center falls in the region S_1 (shown in Fig. 3), so the *Type* I blockage area $S_{T1}(w,l,\theta)$ can be calculated as:

$$S_1(w,l,\theta) = R_1 \cdot (l \cdot \sin\theta + w \cdot \cos\theta) + C_1 \cdot l^2 + C_2 \cdot l \cdot w - C_3 \cdot w^2, \tag{3}$$

where R_1 is the length of original link L_1, which equals d_w/sinθ, $\gamma = \theta$ - actan[(tan θ)/3)], and C_1, C_2, C_3 are

$$\begin{cases} C_1 = \frac{1}{4} \cdot \sin 2\theta - \frac{1}{2} \cdot \cot\gamma \cdot \sin^2\theta \\ C_2 = \frac{1}{2}(\cos 2\theta - \cot\gamma \cdot \sin 2\theta) \\ C_3 = \frac{1}{4} \cdot \sin 2\theta + \frac{1}{2} \cdot \cot\gamma \cdot \cos^2\theta + \frac{1}{8}\cot\theta. \end{cases} \tag{4}$$

A *Type* II blockage blocks both the original link L_1 and the adjacent longer alternative link L_3 at the same time, which means that the center of an arbitrary rectangle falls in the region $S_{1,2}$, and the blockage area $S_{T2}(w,l,\theta)$ is obtained as:

$$S_{1,2}(w,l,\theta) = C_4 \cdot w^2 + C_5 \cdot l \cdot w - C_1 \cdot l^2, \tag{5}$$

where

$$\begin{cases} C_4 = \frac{1}{2} \cdot \cos^2\theta \cdot \cot\gamma - \frac{1}{4} \cdot \sin 2\theta - \frac{1}{2}\cot\theta \\ C_5 = \frac{1}{2} \cdot \sin 2\theta \cdot \cot\gamma - \frac{1}{2}\cos 2\theta. \end{cases} \tag{6}$$

Fig. 4 shows the *Type* III blockage area, where if the center of a random rectangle falls in the region $ABCD$ ($S_{1,3}$), both an original link L_1' and a crossed diagonal alternative link L_3 will be blocked simultaneously. The corresponding blockage area $S_{T3}(w,l,\theta)$ is:

$$S_{1,3}(w,l,\theta) = \frac{l^2 \sin(\theta-\gamma)\sin\theta}{\sin(2\theta-\gamma)} + \frac{w^2\cos(\theta-\gamma)\cos\theta}{\sin(2\theta-\gamma)} + l \cdot w. \tag{7}$$

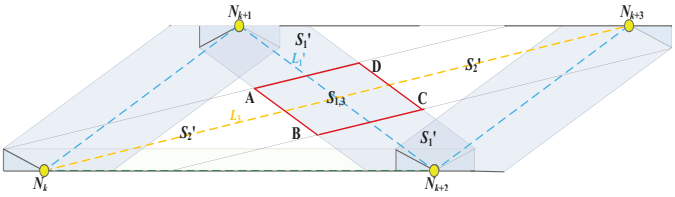

Fig. 4. Spatial correlation of the crossed link and original link.

The occurrence of *Type* IV blockage indicates all TX/RX links of one node (e.g. L_1, L_2 and L_3 shown in Fig. 3) are blocked, i.e., a random rectangle intersects these three links simultaneously when its center falls in the area $S_{1,2,3}$. The *Type* IV blockage area $S_{T4}(w,l,\theta)$ is computed as:

$$S_{1,2,3}(w,l,\theta) = \frac{3}{8} \cdot w^2 \cdot \cot\theta + \frac{1}{2} \cdot w \cdot l. \tag{8}$$

From the above analyses, according to the uniform distribution of the random obstacle, the different-type blockage probabilities P_{Ti} ($1 \le i \le 4$) can be derived as $P_{Ti} = S_{Ti}(w,l,\theta)/A(w,l,\theta)$ in the single-obstacle case, where $A(w,l,\theta)$ is the area of the entire link region.

B. Multi-obstacle cases

Due to the correlation of random obstacles, the multi-obstacle cases can not be simply viewed as a sum of multiple single-obstacle cases. For example, the *Type* II blockage only occurs when a center of obstacle falls in the blockage area $S_{1,2}$ (shown in the Fig. 3) in single-obstacle cases, however, for multi-obstacle cases, it can also be produced under the situation that a center of one obstacle falls in the area S_1 and a center of another obstacle falls in the area S_2 simultaneously. For this reason, we make another reasonable assumption for the multi-obstacle analysis.

Assumption 3: Obstacles are assumed to form a Boolean scheme of rectangles. The centers C_o of these rectangles fall within the road, and form a homogeneous Poisson point process (PPP) of density λ. The widths W_o and lengths L_o are assumed to be i.i.d. distributed and follow the normal

distribution as $N(\mu_w,\ {\sigma_w}^2)$ and $N(\mu_l,\ {\sigma_l}^2)$. The orientation θ_o of every obstacle is the same as road's direction (i.e., $\theta_o = \theta$). In this way, each obstacle $B(w,l,\theta)$ is completely characterized by the quadruple $\{C_o, W_o, L_o, \theta\}$.

According to the Poisson distribution property, the number of obstacles occurring in disjoint areas are independent. Thus we divide the entire blockage area into following disjoint areas $\{S_1, S_{1,2}, S_{1,2,3}, S_2, S_{2,3}, S_3\} \in \mathbf{S}_i$ (shown in the Fig. 3), and if the center of an obstacle falls in one of these areas, the corresponding link L_i is disconnected. In this way, we start to find the distribution of the number of blockages.

First, let $N(w,l,\theta)$ be the number of obstacles, which fall in the blockage area S_i and cross the link L_i. According to the definition of spatial Poisson point process, if the points belong to a homogeneous PPP with parameter $\lambda > 0$, the probability of k points existing in S_i is given by:

$$P\{N(S_i) = k\} = \frac{(\lambda \cdot |S_i|)^k}{k!} \exp(-\lambda \cdot |S_i|). \tag{9}$$

Thus $N(w,l,\theta)$ is a Poison variable with mean $E[N(w,l,\theta)]$ = $\lambda_{w,l,\theta} \cdot S_i(w,l,\theta)$, where $\lambda_{w,l,\theta} = \lambda \cdot f_W(w)dw f_L(l)dl$.

Second, let *K* be the total number of obstacles with random sizes that fall in their respective blockage areas S_i, and $K(S_i) = \sum_{w,l,\theta} N(w,l,\theta)$. With the superposition theorem of the Poisson point process, which indicates that the superposition of independent Poisson point processes $N_i(w,l,\theta)$ with mean measures Λ_i will still be a Poisson point process with mean measure $\Lambda = \sum_i \Lambda_i$, therefore, *K* is also Poisson distributed, and its expectation can be calculated as:

$$\Lambda_{S_i} = \int_W \int_L \lambda \cdot S_i(w,l,\theta) \cdot f_L(l) \cdot f_W(w) dw dl. \tag{10}$$

Then the probability of *k* random obstacles fall in S_i can be derived as $P\{K(S_i) = k\} = \frac{(\Lambda_{S_i})^k}{k!} \exp(-\Lambda_{S_i})$. Therefore, the probability that no obstacles exist in the area S_i is $P\{K(S_i) = 0\} = \Pr(\overline{S_i}) = \exp(-\Lambda_{S_i})$, conversely, the probability that at least one random obstacle occurs in S_i (i.e., the corresponding link L_i is blocked) is $\Pr(S_i) = 1 - \exp(-\Lambda_{S_i})$.

According to Eq. (3)–(8) and (10), we can derive the expectation of the number of obstacles Λ_{S_i} for each disjoint blockage area in $\mathbf{S}_i$ as Eq. (11)–(17):

$$\begin{aligned}\Lambda_{S_1} = \lambda \cdot [&(\mu_l \cdot \sin\theta + \mu_w \cdot \cos\theta) \cdot R_1 + C_1 \cdot (\mu_l^2 + \sigma_l^2) \\ &+ C_2 \cdot \mu_w \cdot \mu_l - C_3 \cdot (\mu_w^2 + \sigma_w^2)],\end{aligned} \tag{11}$$

$$\Lambda_{S_{1,2}} = \lambda[C_4 \cdot (\mu_w^2 + \sigma_w^2) + C_5 \cdot \mu_w \cdot \mu_l - C_1 \cdot (\mu_l^2 + \sigma_l^2)], \tag{12}$$

$$\begin{aligned}\Lambda_{S_2} = \lambda \cdot [\mu_l \cdot \sin(\theta-\gamma) + \mu_w \cdot \cos(\theta-\gamma)] \cdot R_3 + \lambda \cdot C_1 \\ \cdot (\mu_l^2 + \sigma_l^2) + \lambda \cdot C_6 \cdot (\mu_w^2 + \sigma_w^2) + \lambda \cdot C_7 \cdot \mu_l \cdot \mu_w,\end{aligned} \tag{13}$$

where C_6, C_7 are described in Eq. (14), and R_3 is the length of longer-substitute link L_3, which equals $d_0 \cdot \sqrt{\tan^2\theta + 9}$.

$$\begin{cases} C_6 = \frac{1}{4} \cdot \sin 2\theta - \frac{1}{2} \cdot \cos^2\theta \cdot \cot\gamma - \frac{5}{8}\cot(\theta-\gamma) \\ C_7 = \frac{1}{2}\cos 2\theta - \frac{1}{2} \cdot \sin 2\theta \cdot \cot\gamma - 1, \end{cases} \tag{14}$$

$$\Lambda_{S_{2,3}} = \frac{3}{8} \cdot \lambda \cdot \cot(\theta-\gamma) \cdot (\mu_w^2 + \sigma_w^2) + \frac{3}{8} \cdot \lambda \cdot \mu_l \cdot \mu_w, \tag{15}$$

$$\Lambda_{S_{1,2,3}} = \tfrac{3}{8} \cdot \lambda \cdot \cot\theta \cdot (\mu_w^2 + \sigma_w^2) + \tfrac{1}{2} \cdot \lambda \cdot \mu_w \cdot \mu_l, \tag{16}$$

$$\Lambda_{S_3} = \lambda \cdot \{\frac{1}{2}\mu_w \cdot R_2 - \frac{3}{8}[\cot\theta + \cot(\theta-\gamma)](\mu_w^2 + \sigma_w^2) - \frac{1}{2}\mu_l \cdot \mu_w\}, \tag{17}$$

where $R_2 = 2 \cdot d_0$ is the length of shorter-substitute link L_2.

From Fig. 4 and referring to Eq. (7), the expectation $\Lambda_{S_{1,3}}$ of $K(S_{1,3})$ can be derived as:

$$\begin{aligned}\Lambda_{S_{1,3}} = &\tfrac{\lambda \cdot \sin\theta \cdot \sin(\theta-\gamma)}{\sin(2\theta-\gamma)} \cdot (\mu_l^2 + \sigma_l^2) + \tfrac{\lambda \cdot \cos\theta \cdot \cos(\theta-\gamma)}{\sin(2\theta-\gamma)} \\ &\cdot (\mu_w^2 + \sigma_w^2) + \lambda \cdot \mu_w \cdot \mu_l.\end{aligned} \tag{18}$$

From the results above, in one original link region, the occurrence probability of *Type* I blockage P_I, i.e., the probability that both alternative links L_2 and L_3 are available but the original link L_1 is blocked, can be calculated as:

$$\begin{aligned}&\Pr(L_2 \cdot L_3 \cdot \overline{L_1}) \\ &= \Pr\{\overline{S_1 \cdot S_{1,2,3} \cdot S_{1,2}} \cdot (S_2 \cdot S_{2,3} \cdot S_{1,2,3}) \cdot (S_3 S_{1,2,3} S_{2,3})\} \\ &= \Pr\{(\overline{S_1} + \overline{S_{1,2,3}} + \overline{S_{1,2}}) \cdot S_2 \cdot S_{2,3} \cdot S_{1,2,3} \cdot S_{1,2} \cdot S_3\} \\ &= \Pr(\overline{S_1} \cdot S_2 \cdot S_{2,3} \cdot S_{1,2,3} \cdot S_{1,2} \cdot S_3) \\ &\overset{(a)}{=} \prod_{i \neq 1} \Pr(\overline{S_1}) \cdot \Pr(S_i) \\ &\overset{(b)}{=} (1 - e^{-\Lambda_{S_1}}) \cdot e^{-(\Lambda_{S_2} + \Lambda_{S_{2,3}} + \Lambda_{S_{1,2,3}} + \Lambda_{S_{1,2}} + \Lambda_{S_3})}.\end{aligned} \tag{19}$$

Here, (a) is true because the events where centers of obstacles fall in different non-overlapping blockage areas are independent, and (b) follows from the basic property of homogeneous Poisson distribution with density λ. Taking Eq. (11)–(17) into Eq. (19), we can get the expression of occurrence probability of *Type* I blockage.

In the same way, the *Type* II blockage probability P_{II} is derived as:

$$\begin{aligned}&\Pr(\overline{L_1} \cdot \overline{L_3} \cdot L_2) \\ &= \Pr\{\overline{S_1 S_{1,2,3} S_{1,2}} \cdot (\overline{S_2 S_{2,3} S_{1,2,3} S_{1,2}})(S_3 S_{1,2,3} S_{2,3})\} \\ &\overset{(c)}{=} [1 - e^{-(\Lambda_{S_1} + \Lambda_{S_2})} - e^{-(\Lambda_{S_2} + \Lambda_{S_{1,2}})} + e^{-(\Lambda_{S_1} + \Lambda_{S_2} + \Lambda_{S_{1,2}})}] \\ &\quad \cdot e^{-(\Lambda_{S_{1,2,3}} + \Lambda_{S_{2,3}} + \Lambda_{S_3})},\end{aligned} \tag{20}$$

where (c) follows from the inclusion-exclusion principle and homogeneous Poisson distribution property.

Referring to Fig. 4, the *Type* III blockage probability P_{III} can be derived with the similar analysis as follow:

$$\begin{aligned}&\Pr(\overline{L_1{}'} \cdot \overline{L_3}) = \Pr\{\overline{S_1{}' \cdot S_{1,3}} \cdot \overline{S_2{}' \cdot S_{1,3}}\} \\ &= \Pr\{(\overline{S_1{}'} + \overline{S_{1,3}}) \cdot (\overline{S_2{}'} + \overline{S_{1,3}})\} \\ &\overset{(b)}{=} (1 - e^{-\Lambda_{S_1'}}) \cdot (1 - e^{-\Lambda_{S_2'}}) + 1 - e^{-\Lambda_{S_{1,3}}} - (1 - e^{-\Lambda_{S_1'}}) \\ &\quad \cdot (1 - e^{-\Lambda_{S_2'}}) \cdot (1 - e^{-\Lambda_{S_{1,3}}}),\end{aligned} \tag{21}$$

where $\Lambda_{S_1'} = \lambda \cdot (\mu_l R_1 \sin\theta + \mu_w R_1 \cos\theta - \frac{1}{4}(\mu_w^2 + \sigma_w^2)\cot\theta - \Lambda_{S_{1,3}}$, and $\Lambda_{S_2'} = \lambda \cdot [R_3 \cdot \sin(\theta-\gamma) \cdot \mu_l + R_3 \cdot \cos(\theta-\gamma) \cdot \mu_w - \frac{1}{4} \cdot \cot(\theta-\gamma) \cdot (\mu_w^2 + \sigma_w^2)] - \Lambda_{S_{1,3}}$.

The derivation of *Type* IV blockage probability $\Pr(\overline{L_1} \cdot \overline{L_2} \cdot \overline{L_3})$ is not straightforward since there would be many items after using inclusive-exclusion principle, but we can first compute $\Pr(\overline{L_1})$ and the conditional probability $\Pr(\overline{L_2} \cdot \overline{L_3} | \overline{L_1})$ respectively as follow:

$$\Pr(\overline{L_1}) = 1 - e^{-(\Lambda_{S_1}+\Lambda_{S_{1,2}}+\Lambda_{S_{1,2,3}})} = 1 - e^{-\lambda\cdot[R_1\cdot\sin\theta\cdot\mu_l + R_1\cdot\cos\theta\cdot\mu_w - \frac{1}{4}\cdot\cot\theta\cdot(\mu_w^2+\sigma_w^2)]}, \quad (22)$$

$$\Pr(\overline{L_2}\cdot\overline{L_3}|\overline{L_1}) = 1 - \Pr(\overline{\overline{L_2}\cdot\overline{L_3}}|\overline{L_1}) = 1 - \frac{\Pr(L_2\cdot\overline{L_1})+\Pr(L_3\cdot\overline{L_1})-\Pr(\overline{L_1}\cdot L_2\cdot L_3)}{\Pr(\overline{L_1})} \overset{(c)}{=} 1 - [1 - e^{-\Lambda_{S_1}-\Lambda_{S_{1,2}}-\Lambda_{S_{1,2,3}}}]^{-1}\{e^{\sum_{i\neq 1;3}-\Lambda_{S_i}}(1-e^{-\Lambda_{S_1}})\cdot(1-e^{-\Lambda_{S_3}}) + e^{-(\Lambda_{S_3}+\Lambda_{S_{2,3}}+\Lambda_{S_{1,2,3}})}\cdot[1-e^{-(\Lambda_{S_1}+\Lambda_{S_{1,2}})}]\}. \quad (23)$$

Then it is easy to get *Type* IV blockage probability P_{IV} by $\Pr(\overline{L_1}\cdot\overline{L_2}\cdot\overline{L_3}) = \Pr(\overline{L_2}\cdot\overline{L_3}|\overline{L_1})\cdot\Pr(\overline{L_1})$.

IV. Parametric Analysis on Blockage Probability

Based on the preceding theoretical analysis of blockage effects in the IFTW topology, we know the different-type blockage probabilities as a function of the topology and obstacle parameters. Here, we investigate how these parameters affect the blockage robustness in a specific roadside scenario.

A. The impact of different parameters on blockage probability

Assuming that the IFTW topology is deployed along the roadside environment, where the road width is $d_w = 16$m, and the obstacle density λ is set as 6.25×10^{-4} m^{-2} (about one obstacle every 100m on the road). For the large vehicles as obstacles on the road, their widths and lengths are normally distributed as $\mathcal{N}(\mu_w$=2.3, σ_w=0.8) and $\mathcal{N}(\mu_l$=8.0, σ_l=2.5). In this scenario, all parameters of obstacles including the expected size and density are known, and the blockage probability is evaluated as a function of the topology angle θ, thus we can choose a topology angle that reduces the blockage probability to an acceptable value.

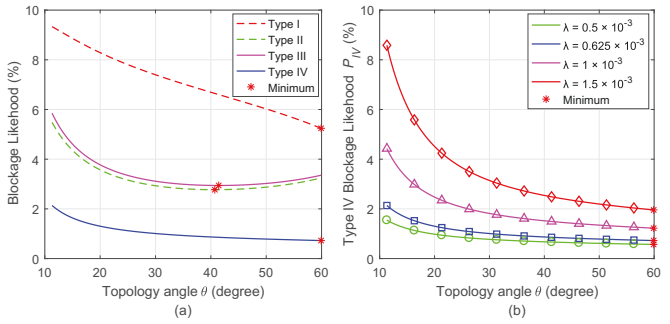

Fig. 5. The different-type blockage probabilities vs. topology angle.

Fig. 5 shows blockage likelihoods vs. the topology angle. Fig. 5(a) shows clearly that *Type* I blockages are the most likely type to be produced by random obstacles. It also shows that, while *Type* I and IV blockage probabilities are monotonically decreasing as θ increases, *Type* II and III blockage probabilities are minimized at an intermediate value of θ.

We know that *Type* IV blockages have the most severe impact. Fig. 5(b) shows the *Type* IV blockage probability vs. θ for different obstacle densities. From Fig. 5(b), we can see that as the obstacle density increases, *Type* IV blockage probability also increases, but the minimum (less than 2%) is always obtained when choosing the largest topology angle θ.

In addition to the topology parameters, the sizes of random obstacles also impact the blockage probabilities. Here, we determine a specific topology with $\theta = 15°$, which satisfies the interference-free condition (Eq. 1) with $\phi = 15°$. In Fig. 6, as μ_l (with the fixed μ_w=2.3) and μ_w (with the fixed μ_l=8.0) vary, respectively, we can see that different-type blockage probabilities increase when the obstacle's size becomes larger. The likelihood of *Type* IV blockages, which are the most likely to cause communication outage, increases more rapidly with the obstacle's width than with the length.

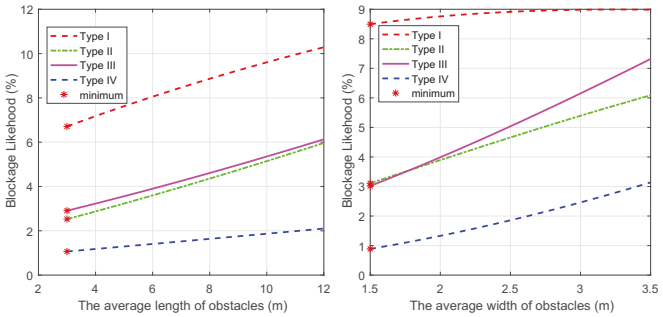

Fig. 6. Blockage Probability vs. average length and width of obstacle.

B. Modification of the IFTW topology

According to the high-throughput path reconfiguration algorithm (HTPR) for blockage avoidance in our previous paper [5], it is known that *Type* I blockages can always be handled, and most of the cases where reconfiguration fails are caused by *Type* IV blockages that occur very close to the source or destination BS (Theorem 2 in [5]). From Fig. 5 (b), we know that the *Type* IV blockage probability in one link region decreases rapidly as the topology angle θ increases. To improve the blockage robustness of the IFTW topology, one idea is to increase the near-BS topology angles (i.e., θ_0 and θ_{N-2} in the first and last link region) but keep the other angles θ_i $(1 \le i \le N-3)$ at smaller values that satisfy the interference-free condition in order to minimize the number of deployed relay nodes. This modified topology, which we refer to as the wide-end-angle IFTW (WEA-IFTW) topology is shown in Fig. 7. Although it is difficult to derive the outage probability analytically for this complete topology, we will investigate its blockage robustness through simulation and compare it against the IFTW topology.

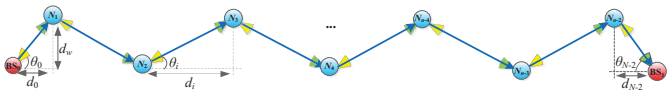

Fig. 7. The WEA-IFTW topology.

Theorem 1. *The WEA-IFTW topology is interference-free if all angles satisfy the interference-free condition in Eq. 1.*

Proof. It is known that the original IFTW topology becomes interference-free when each angle θ_i satisfies the interference-free condition, i.e. $\theta_i - \arctan(\frac{\tan\theta_i}{3}) > \frac{\phi}{2}$. Now considering the first link region without mutual interference from other link regions, the inequality $\gamma = \theta_0 - \arctan(\frac{1}{\cot\theta_0 + 2\cot\theta_i}) > \frac{\phi}{2}$ $(\theta_0 \ge \theta_i)$ should be satisfied. Since γ monotonically increases as θ_0 increases, γ_{min} is obtained when $\theta_0 = \theta_i =$

$\arctan[(\tan\theta_i)/3]$, and $\gamma_{min} > \phi/2$, therefore, γ is always greater than $\frac{\phi}{2}$, and the original interference-free condition holds. Due to the symmetry of the topology, the same result can be easily obtained in the last link region. □

In the IFTW topology, we refer to the communication loss caused by the near-BS *Type* IV blockages as the *near-BS outage*, and the near-BS outage probability P_{otg} is reduced as the *Type* IV blockage probability decreases. Since the first and last link regions are disjoint along the multi-hop relays, we can derive $P_{otg} = 1 - (1 - P_{IV})^2$.

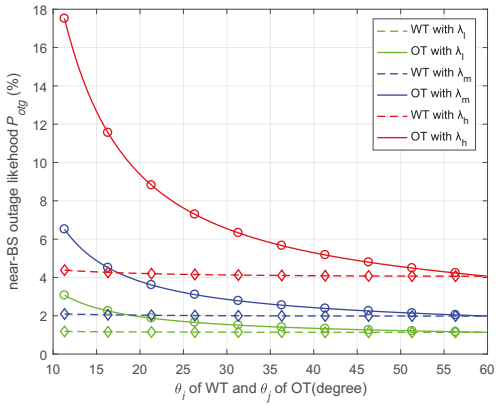

Fig. 8. The near-BS outage probability vs. topology angles.

Fig. 8 shows the near-BS outage probability comparison between the IFTW topology (OT) and the WEA-IFTW topology (WT). In OT, the topology angles θ_j $(0 \le j \le N-2)$ are the same everywhere. As for WT, the near-BS topology angle θ_0 and θ_{N-2} are set at specific larger values (60°), while other elevation angles θ_i $(1 \le i \le N-3)$ stay the same. It is clear that the outage probability decreases substantially in WT compared with OT for different levels of obstacle density (high density $\lambda_h = 1.56 \cdot 10^{-3}$, medium density $\lambda_m = 0.83 \cdot 10^{-3}$ and low density $\lambda_l = 0.5 \cdot 10^{-3}$). Especially when choosing the smaller angles under the high-density obstacle condition, there is about 75% reduction in the outage probability in WT. In addition, the near-BS outage probability of WT is almost unchanged as θ_i varies, thus it is more appropriate to select the smaller θ_i in WT, which aims to minimize the number of relay nodes and meet the high-throughput requirement as well, and does not affect blockage robustness at the same time.

Although the blockage robustness is improved, as a trade-off, the WEA-IFTW topology leads to deploying additional relays to cover the same length of the road. Here, we make a conclusion about the number of additional relays in the WT.

Theorem 2. *Under the principle of deploying the minimum number of relays in the topology (i.e., $\theta_i = \theta_j$ with the smallest values satisfying Eq. 1), at most two additional relays need to be deployed in the WEA-IFTW topology, and only one additional relay is required when the near-BS topology angle θ_k (k=0, N-2) and other topology angles θ_i (1≤i<N-3) satisfy the following condition:*

$$\theta_i < \theta_k \le \arctan(2 \cdot \tan\theta_i). \tag{24}$$

Proof. From Fig. 7, to cover the same length of the road as OT, the extra distance is $\triangle d = 2 \cdot (d_w/tan\theta_i - d_w/tan\theta_k)$. We know that one separated distance $d_w/tan\theta_i$ leads to one additional relay node, and the number of required additional relays will not be larger than two since $0 < \triangle d < 2 \cdot d_w/tan\theta_i$. On the other hand, when $\triangle d \le d_w/tan\theta_i$, i.e., the inequality (24) holds, only one more relay is required to be deployed. □

V. Numerical Results

In this section, numerical results are provided to evaluate network performance and verify our mathematical analyses. We assume the HTPR algorithm is used for blockage avoidance [5], where shorter alternative links are more likely to be selected for avoiding different-type blockages. Then, we place a number of random obstacles along the roadway, and evaluate the end-to-end throughput and blockage tolerance rate (BTR). We make use of the optimal scheduling algorithm of [4] and the channel model of Sec. II to calculate the end-to-end throughput. BTR is 100% if the HTPR algorithm can handle the blockage, otherwise it is reduced to zero.

All evaluations are done at the mmWave frequency of 60 GHz with a 2.16 GHz bandwidth. The directional antenna gains G_t, G_r of each wireless node are 25 dBi and the transmit power is 1 watt. The attenuation from oxygen absorption is 17 dB/km, and a 15 dB link margin that covers the rain attenuation and noise figure is considered. Here we investigate the WEA-IFTW topology both with and without additional relays (as compared to the original IFTW topology) in a roadside environment, where the road width d_w is 18m and road length d_l is about 1km.

A. With additional relays

In this part, we evaluate the network performance in the following two scenarios, where obstacles are generated randomly in the topology and are handled by the HTPR algorithm. Every random obstacle's width and length are normally distributed as $\mathcal{N}(\mu_w$=2.3, σ_w=0.8) and $\mathcal{N}(\mu_l$=8.0, σ_l=2.5).

Scenario 1: The original IFTW topology is considered, with each topology angle θ_j set as 11.7°, which is small enough to minimize the number of relay nodes while satisfying the interference-free condition (with $\phi = 15°$). To cover the whole length of the road, 10 regular-spaced relay nodes need to be deployed along the roadside.

Scenario 2: The WEA-IFTW topology is considered, where the near-BS angles θ_0 and θ_{N-2} are set as a larger value (60°), and other topology angles θ_i $(1 \le i \le N-3)$ are the same as Scenario 1 (11.7°). In this way, compared to Scenario 1, two additional relays are required to cover the entire road.

From Fig. 9(a), we can see that the BTRs of both scenarios decrease as the obstacle density increases since more blockages are produced. For obstacle densities of at most $\lambda \le 3 \times 10^{-4}$ (i.e., fewer than 6 obstacles that affect original links on the road), both Scenario 1 and Scenario 2 have good blockage tolerance. However, when obstacle density is higher, the BTR of Scenario 1 drops fairly rapidly, while Scenario 2 still shows a good BTR (more than 80%). This result verifies that the near-BSs *Type* IV blockage is a key factor, because by adjusting the near-BS angle in the WEA-IFTW topology (Scenario 2), the BTR can be improved by more than 28% compared with the original IFTW topology.

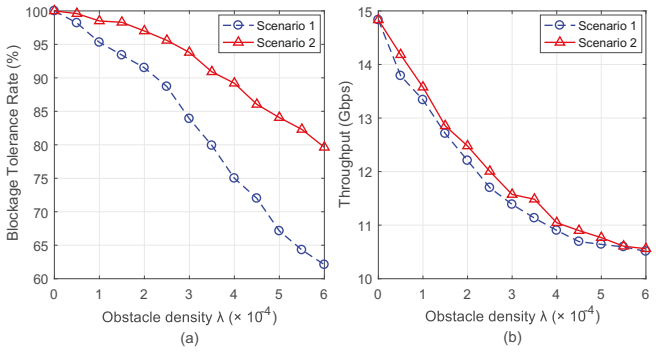

Fig. 9. Performance comparisons in different scenarios.

In addition, we also compare the average end-to-end throughputs (computed only over successful reconfiguration cases). As shown in Fig. 9(b), since more bottleneck links are selected for blockage avoidance when higher obstacle density is allowed, the throughputs decrease gradually, however, they can still meet the high-throughput backhaul requirement (over 10+ Gbps). Compared to Scenario 1, the throughput is even a little higher in Scenario 2. That is because the alternative links of the near-BS regions become shorter after adjustment, and once they are selected as bottleneck links for blockage avoidance, it would result in a higher average throughput.

From above, we can see that the WEA-IFTW topology has advantages in both blockage robustness and throughput, but as a trade-off, two additional relay nodes are required. Note that if θ_0 and θ_{N-2} are adjusted as 22° in Scenario 2, which satisfies the inequality (24) in Theorem 2, we only need to deploy one additional relay.

B. Without additional relays

In order to avoid deploying additional relays with WEA-IFTW topology, one method is to equip directional antennas with narrower beamwidth in each wireless node, thus we can adopt the smaller topology angle θ_i according to Eq. (1). In this way, all the original link lengths (except the first and last original link) would be stretched to make the number of required relays stay unchanged.

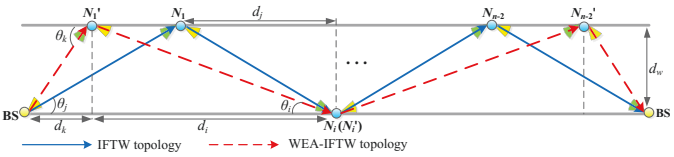

Fig. 10. IFTW topology and WEA-IFTW topology with no additional relays.

As Fig. 10 shows, the IFTW topology is established along the roadside, where the antenna beamwidth of each node ϕ = 15°, every topology angle θ_j = 11.7°, and d_j = 87m. For the WEA-IFTW topology, every antenna beamwidth ϕ' is reduced to 12°, so that the topology angle θ_i can be set as 9.7° ($1 \leq i \leq N-3$), which satisfies the interference-free condition. In addition, the near-BS topology angle θ_k is increased to 60°, and d_k = 10.4m and d_i = 105.3m. In this way, the number of deployed relays is 10 in both topologies.

From Fig. 11(b), we can see that the throughput degrades a little in the WEA-IFTW topology. This is because most links are stretched a little to maintain the same number of deployed relays. However, this throughput can still be around 10 Gbps even if a number of obstacles occur. In addition, due to the larger near-BS topology angles, the blockage robustness has an obvious improvement for the WEA-IFTW topology (shown in Fig. 11(a)), where the BTR is increased by about 25%.

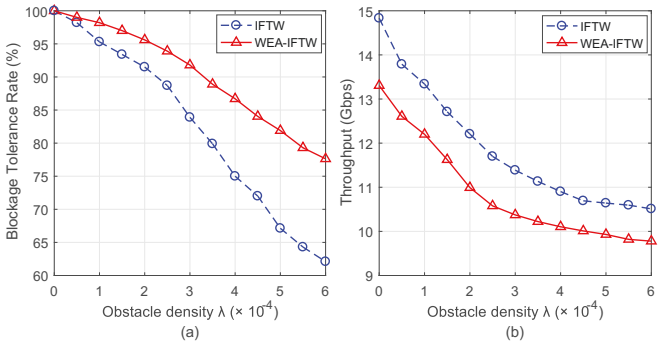

Fig. 11. Performance comparisons between two topologies.

VI. Conclusion

In this paper, we studied blockage effects in roadside relay-assisted mmWave backhaul networks, and derived blockage probabilities for different blockage types, which shows that blockage robustness is significantly impacted by the near-BS topology angles. Numerical results show that adjustment to near-BS angles of the topology results in a substantial improvement of robustness, and can still support required throughputs without increasing the number of deployed relays.

Acknowledgement

This research was supported in part by the National Science Foundation through Award CNS–1813242.

References

[1] J. Du, et al.,"Gbps user rates using mmWave relayed backhaul with high gain antennas", *IEEE Journal on Selected Areas in Comm.*, 2017.

[2] R. Rony, et al.,"Joint access-backhaul perspective on mobility management in 5G networks", *IEEE Comm and Netw* (CSCN), 2017.

[3] T. Bai, and H. Robert, "Coverage analysis for millimeter wave cellular networks with blockage effects", *IEEE GlobalSIP*, 2013.

[4] Q. Hu and D. Blough, "Relay Selection and Scheduling for Millimeter Wave Backhaul in Urban Environments", *Proc. of IEEE International Conference on Mobile Ad-hoc and Sensor Systems*, 2017.

[5] Y. Liu, Q. Hu, and D. Blough, "Blockage Avoidance in Relay Paths for Roadside mmWave Backhaul Networks", *IEEE PIMRC*, 2018.

[6] S. Biswas, S. Vuppala, et al, "On the performance of relay aided millimeter wave networks", *IEEE J. Sel. Topics Signal Process.*, 2016.

[7] Y. Niu, et al, "Blockage robust and efficient scheduling for directional mmWave WPANs", *IEEE Transactions on Vehicular Technology*, 2015.

[8] Z. Liu, et al, "Opportunistic relay selection and outage performance analysis for 60GHz wireless system", *IEEE Globecom Workshops*, 2013.

[9] T. Bai, H. Robert, "Coverage and rate analysis for millimeter-wave cellular networks", *IEEE Transactions on Wireless CommC*, 2015.

[10] F. Baccelli and X. Zhang, "A correlated shadowing model for urban wireless networks", *IEEE Computer Communications* INFOCOM, 2015.

[11] S. Singh, M. Kulkarni, A. Ghosh, et al, "Tractable model for rate in self-backhauled millimeter wave cellular networks", *IEEE Journal on Selected Areas in Communications*, 2015, 33(10): 2196-2211.

[12] T. Bai, R. Vaze, H. Robert, "Analysis of blockage effects on urban cellular networks", *IEEE Transactions on Wireless Comm.*, 2014.

[13] H. Jung and H. Lee, "Outage analysis of multihop wireless backhaul Using millimeter wave under blockage effects", *International Journal of Antennas and Propagation*, 2017.

[14] Q. Hu and D. Blough, "Optimizing Millimeter-Wave Backhaul Networks in Roadside Environments," *Proc. of IEEE ICC*, 2018.